

UC Santa Barbara

UC Santa Barbara Previously Published Works

Title

Cross-plane Seebeck coefficient of ErAs : InGaAs/InGaAlAs superlattices

Permalink

<https://escholarship.org/uc/item/87x5r4fc>

Journal

Journal of Applied Physics, 101(3)

ISSN

0021-8979

Authors

Zeng, G H
Zide, JMO
Kim, W
[et al.](#)

Publication Date

2007-02-01

Peer reviewed

Cross-plane Seebeck coefficient of ErAs:InGaAs/InGaAlAs superlatticesGehong Zeng^{a)}*Department of Electrical and Computer Engineering, University of California, Santa Barbara, California 93106*

Joshua M. O. Zide

Materials Department, University of California, Santa Barbara, California 93106

Woochul Kim

Department of Mechanical Engineering, University of California, Berkeley, California 94720

John E. Bowers

Department of Electrical and Computer Engineering, University of California, Santa Barbara, California 93106

Arthur C. Gossard

Materials Department, University of California, Santa Barbara, California 93106

Zhixi Bian, Yan Zhang, and Ali Shakouri

Electrical Engineering Department, University of California, Santa Cruz, California 95064

Suzanne L. Singer and Arun Majumdar

Department of Mechanical Engineering, University of California, Berkeley, California 94720

(Received 13 July 2006; accepted 29 November 2006; published online 6 February 2007)

We characterize cross-plane and in-plane Seebeck coefficients for ErAs:InGaAs/InGaAlAs superlattices with different carrier concentrations using test patterns integrated with microheaters. The microheater creates a local temperature difference, and the cross-plane Seebeck coefficients of the superlattices are determined by a combination of experimental measurements and finite element simulations. The cross-plane Seebeck coefficients are compared to the in-plane Seebeck coefficients and a significant increase in the cross-plane Seebeck coefficient over the in-plane Seebeck coefficient is observed. Differences between cross-plane and in-plane Seebeck coefficients decrease as the carrier concentration increases, which is indicative of heterostructure thermionic emission in the cross-plane direction. © 2007 American Institute of Physics. [DOI: [10.1063/1.2433751](https://doi.org/10.1063/1.2433751)]

I. INTRODUCTION

Thermoelectric materials can be used for solid state refrigeration and power generation devices. The performance of thermoelectric energy conversion devices depends on the thermoelectric figure of merit (ZT) of a material, which is defined as $ZT = S^2 \sigma T / k$, where S , σ , k , and T are the Seebeck coefficient, electrical conductivity, thermal conductivity, and absolute temperature, respectively. It has been proposed that semiconductor superlattices are a promising thermoelectric material because of (i) enhancement in the power factor ($S^2 \sigma$) due to the quantum confinement effect,¹ (ii) thermal conductivity reduction due to phonon interface scattering,² and (iii) increase in Seebeck coefficient due to thermionic emission.³⁻⁵ So far only the thermal conductivity reduction has been demonstrated^{6,7} conclusively, and much of the recent increase in ZT out of the superlattices^{8,9} comes mainly from the thermal conductivity reduction.¹⁰ However, ZT enhancement due to the power factor increase in a superlattice has not yet been quantified mainly because of the challenge in measuring the cross-plane Seebeck coefficient and cross-plane electrical conductivity. Due to the nonisotropic superlattice structure, the in-plane and cross-plane Seebeck coefficients are usually different. The measurement of in-plane

Seebeck coefficients is straightforward: a temperature difference is built up across a test sample plate, and by measuring the output voltage ΔV at different temperatures ΔT , the Seebeck coefficient of the material can be determined by $\Delta V / \Delta T$. In contrast, the measurement of the cross-plane Seebeck coefficient is challenging because it is difficult to determine the voltage and temperature drop across a thin film superlattice layer only a few microns thick.¹¹⁻¹³ In this paper, we report a method for experimental characterization of cross-plane Seebeck coefficients of superlattice samples by using device test patterns combined with three-dimensional (3D) thermal simulations. Superlattice structures are designed to increase the cross-plane Seebeck coefficient by using heterostructure thermionic emission.³⁻⁵ An explanation of the cross-plane Seebeck coefficient enhancement over in-plane Seebeck coefficient is provided.

II. MATERIAL STRUCTURES

The ErAs:InGaAs/InGaAlAs superlattice samples were grown using a Varian Gen II molecular beam epitaxy system on (100) n -type InP substrates with a buffer layer of 50 nm InGaAs.¹⁴⁻¹⁶ The samples consist of an InGaAs/InGaAlAs superlattice structure with semimetallic ErAs particles randomly distributed through InGaAs layers. The ErAs particles act as a n -type dopant in the InGaAs,¹⁴ and Hall measure-

^{a)}Electronic mail: gehong@ece.ucsb.edu

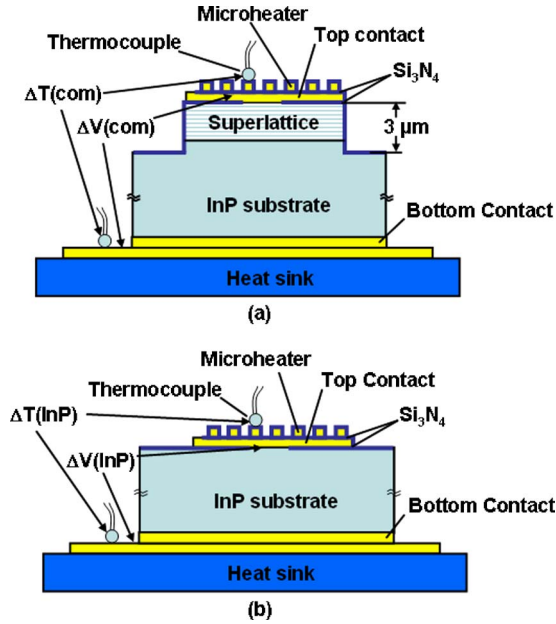


FIG. 1. (Color online) The diagram of the test pattern device structure: (a) integrated microheaters on top of the superlattice mesa and (b) integrated microheaters on the InP substrate.

ments in a van der Pauw geometry show that without codoping, these randomly distributed ErAs particles provide an electron concentration around $2 \times 10^{18} \text{ cm}^{-3}$.¹⁶ The superlattice structure consisted of 70 periods of 10 nm InAlGaAs and 20 nm InGaAs. The silicon codoping values for the four superlattice samples were 0, 2×10^{18} , 4×10^{18} , and $8 \times 10^{18} \text{ cm}^{-3}$, respectively. Both ErAs and Si are electron donors and the total doping values for each sample are 2×10^{18} , 4×10^{18} , 6×10^{18} , and $1 \times 10^{19} \text{ cm}^{-3}$, respectively. The 10 nm InGaAlAs layer consists of a digital alloy of 60% InGaAs and 40% InAlAs, and 0.3% erbium is randomly distributed in the 20 nm *n*-InGaAs layer in addition to silicon codoping. The reason for choosing the combination of these materials to increase *ZT* is described herein. InGaAlAs is known to have a band offset of $\Delta E = 0.2 \text{ eV}$ with respect to ErAs:InGaAs, which could increase the Seebeck coefficient of the sample by approximately $\Delta E/qT$, where q is the charge of an electron. The role of ErAs:InGaAs is to reduce the thermal conductivity below that of InGaAs or InGaAlAs. It has been shown previously that incorporating ErAs nanoparticles 1–5 nm in diameter effectively reduces the thermal conductivity below the InGaAs alloy because ErAs nanoparticles effectively scatter long and midwavelength phonons, while atomic substitution in the InGaAs alloy scatter short wavelength phonons.¹⁷ The hypothesis is that the combination of a large Seebeck coefficient, low thermal conductivity, and possibly high electrical conductivity could potentially increase *ZT*.

III. DEVICE FABRICATION AND MEASUREMENTS

Figure 1 shows the test pattern structure with integrated microheaters on both the top of the superlattice mesa (a) and on the InP substrate (b). A $3 \mu\text{m}$ ErAs:InGaAs/InGaAlAs superlattice mesa was first formed by reactive ion etching, and then the surface was passivated with 300 nm of Si_3N_4 .

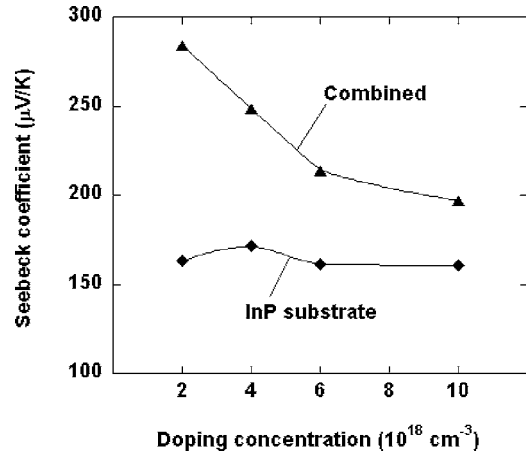


FIG. 2. The combined Seebeck coefficients for the four superlattice samples and the Seebeck coefficients of their InP substrates were measured using device test patterns.

Contact windows were opened on the Si_3N_4 , and a contact metal layer of Ni/GeAu/Ni/Au was deposited via electron beam evaporation. This metal layer is to form Ohmic contact to the semiconductor and the probe electrode as well. Si_3N_4 and SiO_2 double insulating layers of 300 nm thick in total were deposited on top of the contact metal layer, and microheaters of Ti/Au were then patterned on top of the insulating layers. This same pattern was formed on top of the superlattice mesa as well as on the InP substrate. The patterns on top of the superlattice mesa are used for the combined Seebeck coefficient measurement of superlattice and InP substrate, S_{com} , while those on the InP substrate are used for the Seebeck coefficient measurement of the InP substrate, S_{InP} .

When a current flows through the microheater on the top of the InP substrate, a local temperature difference is built up, and the thermoelectric voltage, ΔV_{InP} , and the temperature difference, ΔT_{InP} , between the top contact and the ground contact are simultaneously measured. The InP substrate Seebeck coefficient S_{InP} is the slope of the linearly fitted ΔV_{InP} vs ΔT_{InP} , which is expressed as $S_{\text{InP}} = \Delta V_{\text{InP}}/\Delta T_{\text{InP}}$. Similarly, by using a test pattern on the top of superlattice mesa and a ground electrode on the InP substrate, the temperature difference ΔT_{com} versus output voltage ΔV_{com} can be obtained. The measurement linear fitting value $S_{\text{com}} = \Delta V_{\text{com}}/\Delta T_{\text{com}}$ is a combined Seebeck coefficient, which can be expressed as

$$S_{\text{com}} = S_{\text{SL}} \frac{\Delta T_{\text{SL}}}{\Delta T_{\text{com}}} + S_{\text{InP}} \frac{\Delta T_{\text{InP}}}{\Delta T_{\text{com}}}, \quad (1)$$

where ΔT_{com} is the temperature drop across the superlattice and InP substrate, ΔT_{SL} and ΔT_{InP} are the temperature drop across the superlattice and InP substrate, and S_{SL} is the cross-plane Seebeck coefficient of the superlattice. The measurement results of the InP substrate and combined Seebeck coefficients for the four samples using device test patterns are shown in Fig. 2.

Because there is no direct way to measure the temperature at the interface of the superlattice and InP substrate, a 3D thermal model was built, by which we could estimate the ratio of the temperature drop across the superlattice and the

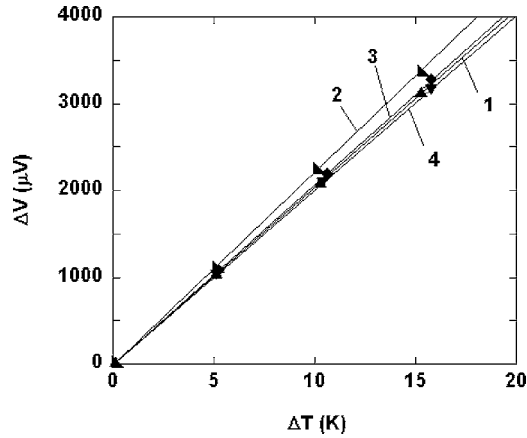


FIG. 3. The lapped InP substrates of the four superlattice samples were measured for the calibration of the results measured using device test patterns, and the Seebeck coefficients were obtained from the slope of the linear fit of the measured ΔV vs ΔT .

InP substrate, $\Delta T_{\text{SL}}/\Delta T_{\text{InP}}$. The thermal conductivity of each individual layer (the ErAs:InGaAs/InGaAlAs superlattice,¹⁸ the InP substrate, and the combined insulating layer of Si_3N_4 and SiO_2) was measured at room temperature using the 3ω technique¹⁹ and used as an input to the simulation. The simulation results show that the temperature difference ratio of $\Delta T_{\text{SL}}/\Delta T_{\text{InP}}$ for the device test patterns is close to 1, therefore by using Eq. (1), the cross-plane Seebeck coefficients for the four ErAs:InGaAs/InGaAlAs superlattice samples with carrier concentrations of 2×10^{18} , 4×10^{18} , 6×10^{18} , and $1 \times 10^{19} \text{ cm}^{-3}$ can be calculated as 405, 326, 265, and 232 $\mu\text{V}/\text{K}$, respectively.

The above measurements assumed that the temperature measured on top of the microheaters was the same as the temperature at the interface of the superlattice surface and contact metal, which should be corrected through calibration. As the transverse and longitudinal masses of the conduction band (Gamma valley) minima of InP substrate are almost the same, the Seebeck coefficients of the InP substrate along the in-plane and cross-plane directions are supposed to be very similar.^{20,21} The calibrations were carried out by removing all the superlattice structures of the four samples and then measuring the Seebeck coefficients of their InP substrates separately. The results were compared with those measured using device test patterns. Each superlattice sample was cut into $5 \times 20 \text{ mm}^2$ in strip size and lapped down about $40 \mu\text{m}$ from the superlattice surface to totally remove the superlattice structures. The indium electrode was patterned at each end of the strip sample. The sample was placed across two separate thermoelectric cooler stages at two different temperatures. The output voltage ΔV and the temperature difference ΔT were measured simultaneously with a multimeter and two thermocouples. Figure 3 shows the linear curve fitting of the measured ΔV vs ΔT , and the Seebeck coefficient values of the four InP substrates for the four superlattice samples with the carrier concentrations of 2×10^{18} , 4×10^{18} , 6×10^{18} , and $1 \times 10^{19} \text{ cm}^{-3}$ are 204, 221, 207, and 200 $\mu\text{V}/\text{K}$, respectively. The slight doping difference in the four different InP substrate samples could result in minor differences among the InP substrate Seebeck coefficients.

By comparing the InP substrate Seebeck coefficients measured using test patterns with the direct measurements using the lapped InP substrate samples, we find that the test pattern measurement results of the four InP substrates are about 20%, 23%, 22%, and 20% less than those of the direct measurements, respectively. The local temperature drops are mainly across the three sections: (i) the insulating Si_3N_4 and SiO_2 layers between the contact metal and the microheater, ΔT_{SiN} , (ii) ErAs:InGaAs/InGaAlAs superlattice layer, ΔT_{SL} , and (iii) InP substrate, ΔT_{InP} . Finite element thermal simulations show that the ratio of $\Delta T_{\text{SiN}}/\Delta T_{\text{InP}}$ is about 1/5 for the InP substrate Seebeck coefficient test pattern shown in Fig. 1(b), and the ratio of $\Delta T_{\text{SiN}}/\Delta T_{\text{SL}}/\Delta T_{\text{InP}}$ is about 1/4.5/4.5 for the combined Seebeck coefficient test pattern shown in Fig. 1(a). When taking the ratio of temperature drop in these three sections into account, the overestimation for ΔT_{InP} in the InP substrate test pattern and ΔT_{com} in the superlattice test pattern is around 20% and 10%, respectively. It was the overestimation of ΔT_{InP} that produced the measurement differences between those using InP test patterns and those using direct measurement methods. Therefore, the cross-plane Seebeck coefficients of the four superlattices with carrier concentrations of 2×10^{18} , 4×10^{18} , 6×10^{18} , and $1 \times 10^{19} \text{ cm}^{-3}$ are 427, 330, 266, and 235 $\mu\text{V}/\text{K}$, respectively, after calibration using Eq. (1) based on the ΔV_{com} and ΔT_{com} measured on test patterns, the Seebeck coefficients of the four InP substrates measured with direct measurement methods, and ratio of temperature drop $\Delta T_{\text{SiN}}/\Delta T_{\text{SL}}/\Delta T_{\text{InP}}$ calculated with finite element thermal simulations.

As our material combination of InGaAs wells with InGaAlAs barriers are designed to enhance the cross-plane Seebeck coefficient by using heterostructure thermionic emission,³⁻⁵ the in-plane and cross-plane Seebeck coefficients are expected to be different. In order to find out this difference, we grew the second set of four 30-period samples of the same superlattice structures and doping concentrations on semi-insulating InP substrates for in-plane Seebeck measurements. The in-plane Seebeck coefficients were measured with the direct measurement method similar to the calibration measurements of those lapped InP substrates described above. The in-plane Seebeck coefficients of 183, 120, 100, and 70 $\mu\text{V}/\text{K}$ were measured for the four samples with carrier concentrations of 2×10^{18} , 4×10^{18} , 6×10^{18} , and $1 \times 10^{19} \text{ cm}^{-3}$, respectively. The measurement results of the in-plane and cross-plane Seebeck coefficients for the two sets of eight samples with different carrier concentrations are shown in Fig. 4.

IV. DISCUSSION

The absolute value of the Seebeck coefficient of a bulk material decreases as the carrier concentration increases and the Fermi level moves deeper into the conduction band.²² This conclusion can be reached from the formula of Seebeck coefficient for a bulk material,

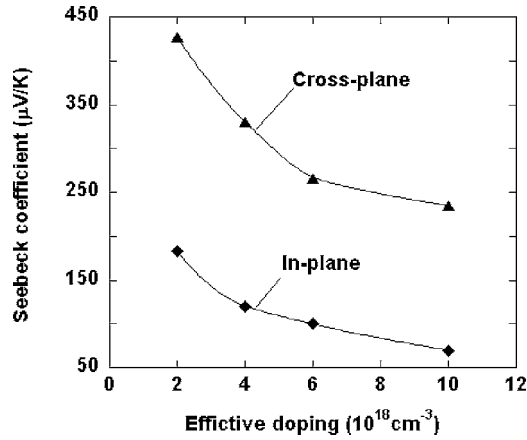


FIG. 4. Measurement results of the cross-plane and in-plane Seebeck coefficients for the two sets of eight ErAs:InGaAs/InGaAlAs superlattice samples.

$$S = \frac{1}{qT} \frac{\int \sigma_d(E)(E - E_F)dE}{\int \sigma_d(E)dE}, \quad (2)$$

where σ_d and E_F are the differential electrical conductivity and Fermi energy, respectively. Usually the same principle can be applied to heterostructures. Both the cross-plane and in-plane Seebeck coefficients of superlattices decrease when the carrier concentration increases. Band diagrams of ErAs:InGaAs/InGaAlAs superlattices were calculated by solving Schrödinger and Poisson equations self-consistently, and the dependence of $E_F - E_C$ on carrier concentration is shown in Fig. 5, where E_C of wells (for in plane) and barriers (for cross plane) are used, respectively.

The enhancement of the Seebeck coefficients in the cross plane over the in-plane direction is obvious in Fig. 4, which results from the energy filtering by potential barriers. When the Fermi level moves deep inside the conduction band of the InGaAlAs barriers, the energy filtering effect is minimal. In this case, the change of the cross-plane Seebeck coefficient with carrier concentrations would be very similar to

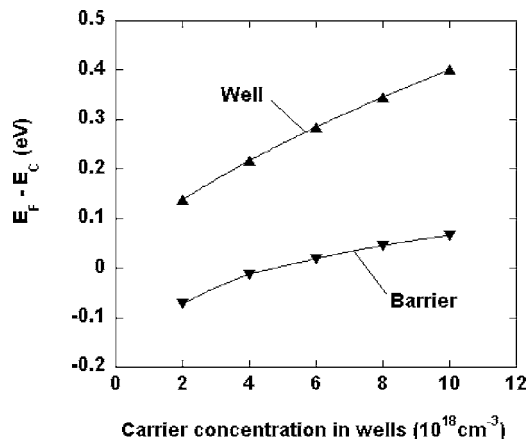


FIG. 5. Calculation results of the energy difference of $E_F - E_C$ for the well and barrier of ErAs/InGaAs superlattice with different carrier concentrations.

that of the in-plane Seebeck coefficient. The experimental results support this reasoning: in the doping range of $2 \times 10^{18} - 4 \times 10^{18} \text{ cm}^{-3}$, the E_F is nearby to E_C for the barriers, and the cross-plane Seebeck coefficient value of Eq. (2) changes more quickly with different carrier concentrations. The differences between the cross-plane and in-plane Seebeck coefficients of the samples with effective dopings of 2×10^{18} and $4 \times 10^{18} \text{ cm}^{-3}$ are 244 and 210 $\mu\text{V/K}$, respectively. When the carrier concentration is over $6 \times 10^{18} \text{ cm}^{-3}$, the Fermi level is deep inside the conduction band for both the wells and barriers, and the integration value rate of change of Eq. (2) with carrier concentrations gradually becomes very similar for both the wells (in plane) and barriers (cross plane). Our measurement results show that the differences of in-plane and cross-plane Seebeck coefficients for the two samples with carrier concentrations of 6×10^{18} and $1 \times 10^{19} \text{ cm}^{-3}$ are very close to each other (Fig. 4), and the differences are 166 and 165 $\mu\text{V/K}$, respectively.

V. CONCLUSION

In summary, a method to measure the cross-plane Seebeck coefficient of a superlattice is described. Two sets of eight ErAs:InGaAs/InGaAlAs superlattice samples with different carrier concentrations were systematically grown and used in this study. We measured combined Seebeck coefficients of the superlattice and the substrate using patterned microheaters. Then, the cross-plane Seebeck coefficients of the superlattice were deduced with the additional information of the temperature difference ratio, $\Delta T_{\text{SL}}/\Delta T_{\text{InP}}$, determined by finite element thermal simulations.

InGaAlAs has a band offset of $\Delta E = 0.2 \text{ eV}$ with respect to ErAs:InGaAs. Therefore, electrons see an energy barrier in the cross-plane direction when the Fermi level is below the conduction band minimum of InGaAlAs. Experimental results showed that there is a significant increase of the cross-plane Seebeck coefficient over the in-plane Seebeck coefficients, and both the cross-plane and in-plane Seebeck coefficients of the superlattices decrease as the carrier concentration increases. The differences between the cross-plane and in-plane Seebeck coefficients decrease with the increase of carrier concentrations. This could indicate heterostructure thermionic emission in the cross-plane direction: as the carrier concentration increases, energy differences, which are related to thermionic emission, between the Fermi level and conduction band minimum of InGaAlAs decrease. Therefore, differences between the cross-plane and in-plane Seebeck coefficients should decrease.

ACKNOWLEDGMENTS

The authors acknowledge useful discussions with Dr. Mihai Gross. This work is supported by the Office of Naval Research Thermionic Energy Conversion Center MURI.

- ¹L. D. Hicks and M. S. Dresselhaus, Phys. Rev. B **47**, 12727 (1993).
- ²M. V. Simkin and G. D. Mahan, Phys. Rev. Lett. **84**, 927 (2000).
- ³A. Shakouri and J. E. Bowers, Appl. Phys. Lett. **71**, 1234 (1997).
- ⁴D. Vashaee and A. Shakouri, J. Appl. Phys. **95**, 1233 (2004).
- ⁵D. Vashaee and A. Shakouri, Phys. Rev. Lett. **92**, 106103 (2004).
- ⁶S. T. Huxtable *et al.*, Appl. Phys. Lett. **80**, 1737 (2002).

- ⁷R. Venkatasubramanian, Phys. Rev. B **61**, 3091 (2000).
- ⁸T. C. Harman, P. J. Taylor, M. P. Walsh, and B. E. LaForge, Science **297**, 2229 (2002).
- ⁹R. Venkatasubramanian, E. Siivola, T. Colpitts, and B. O'Quinn, Nature (London) **413**, 597 (2001).
- ¹⁰G. Chen, A. Narayanaswamy, and C. Dames, Superlattices Microstruct. **35**, 161 (2004).
- ¹¹B. Yang, J. L. Liu, K. L. Wang, and G. Chen, Appl. Phys. Lett. **80**, 1758 (2002).
- ¹²B. Yang, W. L. Liu, J. L. Liu, K. L. Wang, and G. Chen, Appl. Phys. Lett. **81**, 3588 (2002).
- ¹³Y. Zhang, G. Zeng, R. Singh, J. Christofferson, E. Croke, J. E. Bowers, and A. Shakouri, in "Measurement of Seebeck coefficient perpendicular to SiGe superlattice," 21st International Conference on Thermoelectronics, 25–29 August 2002, pp. 329–332.
- ¹⁴D. C. Driscoll, M. Hanson, C. Kadow, and A. C. Gossard, Appl. Phys. Lett. **78**, 1703 (2001).
- ¹⁵D. C. Driscoll, M. P. Hanson, E. Mueller, and A. C. Gossard, J. Cryst. Growth **251**, 243 (2003).
- ¹⁶J. M. Zide, D. O. Klenov, S. Stemmer, A. C. Gossard, G. Zeng, J. E. Bowers, D. Vashaee, and A. Shakouri, Appl. Phys. Lett. **87**, 112102 (2005).
- ¹⁷W. Kim, J. Zide, A. Gossard, D. Klenov, S. Stemmer, A. Shakouri, and A. Majumdar, Phys. Rev. Lett. **96**, 045901 (2006).
- ¹⁸W. Kim *et al.*, Appl. Phys. Lett. **88**, 242107 (2006).
- ¹⁹D. G. Cahill, Rev. Sci. Instrum. **61**, 802 (1990).
- ²⁰S. Adachi, *Physical Properties of III–V Semiconductor Compounds: InP, InAs, GaAs, GaP, InGaAs, and InGaAsP* (Wiley, New York, 1992).
- ²¹I. Kudman and E. F. Steigmeier, Phys. Rev. **133**, A1665 (1964).
- ²²G. Chen and A. Shakouri, ASME Trans. J. Heat Transfer **124**, 242 (2002).